Lubrication of textured surfaces: A general theory for flow and shear stress factors

Michele Scaraggi*
DII, Universita' del Salento, 73100 Monteroni-Lecce, Italy
(Received 18 January 2012; published 23 August 2012)

We report on a mean field theory of textured surface lubrication. We study the fluid flow dynamics occurring at the interface as a function of the texture characteristics, e.g. texture area density, shape and distribution of microstructures, and local slip lengths. The present results may be very important for the investigation of tailored microtextured surfaces for low-friction hydrodynamic applications.

DOI: 10.1103/PhysRevE.86.026314 PACS number(s): 47.85.mf, 47.56.+r, 83.50.Lh

The influence of surface properties on the fluid flow at the interface between solids in stationary or sliding contact is a topic of great importance both in nature and technology. Common applications include leakage of seals, removal of water from the tire-road footprint, and the low-friction lubrication of pairs. Almost all surfaces in nature and most surfaces of interest in tribology present roughness on many different length scales and are often fractal-like, so that when a small region is magnified (in general with different magnifications in the parallel and orthogonal directions) it "looks the same" as the unmagnified surface. This fractal behavior, called "contact splitting" in biomimetic adhesive research, has attracted the attention of a large number of scientists in the past couple of decades and, as a result, the practice of tailoring surface properties by micro (nano-)structures fabrication is nowadays an established research activity [1]. Among those, many applications involve the fluid dynamics occurring over an array of single scale microstructures, such as microholes [2] for low-friction bearings. However, a comprehensive theoretical foundation for sliding texture hydrodynamics is still missing in literature.

In the field of random roughness contact mechanics, most of the fundamental understanding has been recently unified under homogenized contact models, which allow us to effectively capture most of the physics occurring in the wet or dry interactions of real solids [3–8]. In particular, in Refs. [5–8], the authors describe the interface of randomly rough soft contacts as a two-dimensional time-transient porous medium whose network of fluid-filled channels, generally not corresponding to the available amount of interface free volumes, is largely affected by the local fluid-asperity and asperity-asperity interactions [5,6]. Phenomena as percolation islands, roughness anisotropic deformation, and fluid-induced roughness smoothing appear at the interface and strongly determine the contact integral properties, such as friction [5,6].

However, as usually occurs, the process of tailoring surface properties involves the fabrication of ordered one (or at most two-)scale micro (nano-)structures, i.e., the roughness spectral content is effectively quantized. In such cases, as expected, random roughness contact mechanics should not apply due to the different nature of the surface roughness and, therefore, of the contact itself. In the field of fluid flow at confinement, a number of studies has been devoted to the investigation of the role of an array of surface microstructures on the effective fluid flow, wall friction, and slippage [9–11], especially for microfluidic applications. Recently, an increasing attention by researchers has been focused on the manipulation of confined fluids at the interface of (macro-)sliding contacts by means of an ordered lattice of microstructures [2], e.g. with the purpose of minimizing the energy consumption at contact pairs. Observe that, in such applications, the all-fluid dynamics occurring from the micro- to the macroscale has to be calculated in order to determine the macroscopic frictional resistance. From a practical point of view, the numerical resolution of the global fluid dynamics, even in the case of the thin film Reynolds flow, is highly computing demanding and, therefore, not suitable for the estimation (nor for the optimization) of both the local and global effective fluid flow, wall friction, and slippage properties of the sliding contact.

Here we present a homogenized theory for the evaluation of the average texture hydrodynamics in fluids confined at the interface of sliding solids. The model is based on the application of the Bruggeman effective medium [12] (BEM) theory to the thin film Reynolds flow. It allows us to analytically determine the effect of local texture characteristics, e.g. hole ratio and slip length, on the average flow dynamics in terms of correction factors to be included in an effective thin film Reynolds flow equation. The numerical resolution of the latter can be then achieved with a negligible amount of computational efforts if compared to fully deterministic approaches. The model will be then applied to a texture case constituted by a squared lattice of surface holes, and we will compare our model predictions with the numerical (full scale) results obtained by independent research [13].

We consider now the fluid flow at the interface between the solids. We assume that the fluid is Newtonian and that the fluid velocity field $\mathbf{v}(\mathbf{x},t)$ satisfies the Navier-Stokes equation:

$$\frac{\partial \mathbf{v}}{\partial t} + \mathbf{v}\cdot\nabla\mathbf{v} = -\frac{1}{\rho}\nabla p + \nu\nabla^2\mathbf{v},$$

where $\nu = \eta/\rho$ is the kinetic viscosity and ρ the mass density. For simplicity we will also assume an incompressible fluid so that $\nabla\cdot\mathbf{v} = 0$. We assume that the nonlinear term $\mathbf{v}\cdot\nabla\mathbf{v}$ can be neglected (which corresponds to small Reynolds number), which is usually the case of fluid flow between narrowly spaced solid walls. We also assume the lower solid to be rigid with a flat surface, while the upper solid is rigid with an array of microstructures. Moreover, the lower solid moves with the velocity $\mathbf{v}_0$ parallel to the upper (stationary) solid; see Fig. 1.

Let $u(x,y)$ be the separation between the solid walls and assume that $u/L \ll 1$, where L is the linear size of the nominal

*michele.scaraggi@unisalento.it

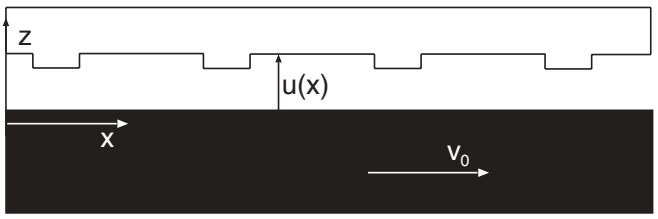

FIG. 1. Schematic (not in scale). A surface-structured solid (block) in contact with a rigid solid (substrate) with a flat surface. The substrate moves with the velocity $\mathbf{v}_0$ while the block is stationary.

contact region. In this case, one expects that the fluid velocity varies slowly with the coordinates x and y as compared to the variation in the orthogonal direction z. Assuming also a slow time dependence the Navier-Stokes equations reduces to:

$$\eta \frac{\partial^2 \mathbf{v}}{\partial z^2} = \nabla p. \tag{1}$$

Here $\mathbf{v} = (v_x, v_y)$, $\mathbf{x} = (x, y)$, and $\nabla = (\partial_x, \partial_y)$ are two-dimensional vectors. Note that $v_z \approx 0$ and that $p(\mathbf{x})$ is independent of z to a good approximation. Of course, in the immediate vicinity of the step walls, Eq. (1) is not applicable; however, we observe that the locally averaged flow properties are not sensibly affected by this approximation in most practical cases [14]. The solution to the equation above can be written, e.g., in the case of no-slip boundary conditions as

$$\mathbf{v} = \frac{1}{2\eta} z[z - u(\mathbf{x})]\nabla p + \left[1 - \frac{z}{u(\mathbf{x})}\right]\mathbf{v}_0, \tag{2}$$

so that $\mathbf{v} = \mathbf{v}_0$ on the solid wall $z = 0$ and $\mathbf{v} = 0$ for $z = u(\mathbf{x})$. Integrating over z [from $z = 0$ to $z = u(\mathbf{x})$] gives the fluid flow vector:

$$\mathbf{J} = -\frac{u^3(\mathbf{x})}{12\eta}\nabla p + \frac{1}{2}u(\mathbf{x})\mathbf{v}_0. \tag{3}$$

More generally, a Navier's boundary condition with slip length l occurs on the microstructure (e.g., because of the presence of local, subinclusion structures allowing for a local Cassie-Baxter regime), resulting in this case:

$$\mathbf{J} = -\left(1 + \frac{3l}{u+l}\right)\frac{u^3}{12\eta}\nabla p + \frac{1}{2}u\left(1 + \frac{l}{u+l}\right)\mathbf{v}_0,$$

where the notation $(\mathbf{x})$ has been suppressed for simplicity. In the case of steady sliding, mass conservation demands that

$$\nabla \cdot \mathbf{J} = 0. \tag{4}$$

Equations (3) and (4) describe the thin film Reynolds flow at the interface between sliding solids. One way to integrate out the surface texture is by using the 2D BEM approach [12,15]. The basic physics behind the effective medium theory is illustrated in Fig. 2. The BEM approach for a thin film Reynolds flow has been originally adopted for the case of static flow through a generally porous medium [16] (i.e., a flow driven by a fluid pressure difference) and more recently for the static flow description of the two-dimensional porous medium

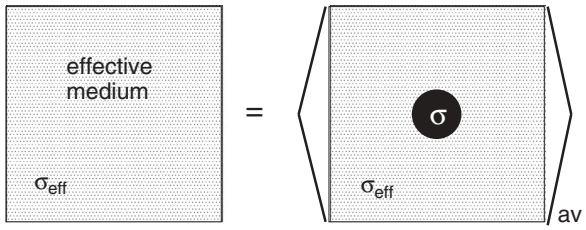

FIG. 2. Schematic. Effective medium theories allow us to describe, at the macroscopic scale, the disorder in a physical system, e.g., fluctuations in the interfacial separation $u(\mathbf{x})$ or in the slip length $l(\mathbf{x})$. For a n-component system (e.g., in the case of an interfacial separation u constituted by n different discrete values) the flow in the effective medium should be the same as the average fluid flow obtained when circular regions of the n-components are embedded in the effective medium.

resulting from the interaction of elastic randomly rough bodies [8]. Here we extend the BEM approach to sliding surfaces.

Consider now the general case of an elliptical homogeneous inclusion in a homogeneous infinite medium, as shown in the draft of Fig. 3. The inclusion represents, e.g., the generic hole (or pillar) of the texturing, and it is characterized by an ellipse semi-major axis aligned with an angle ϕ with respect to the x-reference axis. The infinite medium is instead characterized by a hydraulic (Poiseuille) conductivity $\mathbf{\Lambda}$, which is principally valued in the reference, and by a sliding (Couette) conductivity $\mathbf{\Gamma}$; see Fig. 3. In the easiest case, where the inclusion is represented by a flat ended hole (or pillar) we have $\mathbf{\Lambda}_e = \mathbf{I}\,[1 + 3l_h/(h_h + l_h)]\,h_h^3/(12\eta)$ and $\mathbf{\Gamma}_e = \mathbf{I}\,[1 + l_h/(h_h + l_h)]\,h_h$, where η is the lubricant viscosity, h_h the inclusion height, l_h the local slip length, and $\mathbf{I}$ the identity matrix; see Eq. (3). From Eq. (4), the inclusion lubrication problem can be then formulated as:

$$\nabla \cdot (\mathbf{\Lambda}\nabla p) = \nabla \cdot \bar{Q}, \tag{5}$$

where we have $\bar{Q}$=0 outside the inclusion and $\bar{Q} = -d\mathbf{\Lambda}\nabla p + d\mathbf{\Gamma}U_m = -(\mathbf{\Lambda}_e - \mathbf{\Lambda})\nabla p + (\mathbf{\Gamma}_e - \mathbf{\Gamma})U_m$ elsewhere. $U_m = \mathbf{v}_0/2$ in our case. Equation (5) is subjected to the boundary condition $\nabla p\,(|\mathbf{x}| \to \infty) = \mathbf{\nabla} p_0$ where $\mathbf{\nabla} p_0$ is the

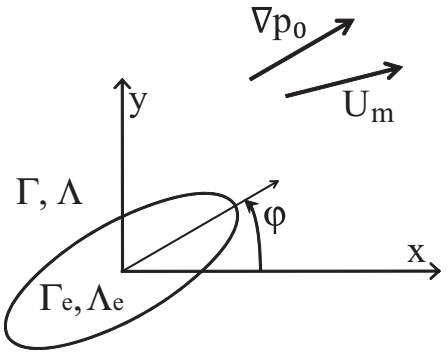

FIG. 3. A generic elliptical homogeneous inclusion immersed in a homogeneous infinite medium. The medium hydraulic conductivity Λ is principally valued in the reference, whereas the medium sliding conductivity Γ is not. ϕ is the ellipse semi-major axis inclination angle. The macroscopic flow driving terms ∇p_0 and U_m are also showed. A Peklenik number $\gamma = a/b$ can be defined as the ratio between the ellipse semi-major axis a and the semi-minor axis b.

externally applied pressure gradient. In the case of static flow, $U_m = 0$ and, therefore, $\bar{Q} = -d\mathbf{\Lambda}\nabla p$ inside the inclusion, resulting in the classical constant polarization vector solution inside the inclusion [16]. However, in our case the inclusion problem can be analytically similarly solved by adopting the following variable change:

$$\nabla p = \nabla f + d\mathbf{\Lambda}^{-1} d\mathbf{\Gamma} U_m. \tag{6}$$

By substituting Eq. (6) in Eq. (5), the resulting inclusion problem is formally equivalent to the static flow case, where this time ∇f is the static flow pressure. Therefore, after integrating Eq. (5) in ∇f, the real pressure gradient ∇p inside the inclusion can be determined:

$$\begin{aligned}\nabla p = &(\mathbf{I} + \mathbf{E}_0 d\mathbf{\Lambda})^{-1} \nabla p_0 \\ &+ [\mathbf{I} - (\mathbf{I} + \mathbf{E}_0 d\mathbf{\Lambda})^{-1}] d\mathbf{\Lambda}^{-1} d\mathbf{\Gamma} U_m,\end{aligned} \tag{7}$$

where the tensorial factor $\mathbf{E}_0 = \int_e d^2\bar{x}\nabla\nabla K$ is a function of the inclusion shape and orientation and of the effective medium hydraulic conductivity. Observe that K is the Green function of the planar orthotropic Laplace equation obtained by solving the two-dimensional problem $\boldsymbol{\nabla} \cdot [\mathbf{\Lambda}\nabla K(x)] = \delta(x)$.

$\int_e d^2\bar{x}\nabla\nabla K = \mathbf{E}_0$ can be calculated in the ellipse reference system. In this case we have

$$\mathbf{E}_0 = [T(\phi)]^t \bar{\mathbf{E}}_0 T(\phi),$$

where $\bar{\mathbf{E}}_0 = \int d^2 x_e [\nabla\nabla K]_{x_e}$ and $T(\phi)$ is the rotation matrix, with $T_{ij}(\phi) = \partial x_i^e / \partial x_j$. After performing the integration we have:

$$\bar{E}_{xx} = \frac{1}{\sqrt{\Lambda_{11}\Lambda_{22}}} \frac{(\sqrt{c_x c_y - d^2} - c_x\gamma)(c_y - c_x\gamma^2) + 2d^2\gamma}{(c_y - c_x\gamma^2)^2 + 4d^2\gamma^2} \tag{8}$$

$$\bar{E}_{yy} = \frac{1}{\sqrt{\Lambda_{11}\Lambda_{22}}} \frac{(\sqrt{c_x c_y - d^2} - c_y\gamma_*)(c_x - c_y\gamma_*^2) + 2d^2\gamma_*}{(c_x - c_y\gamma_*^2)^2 + 4d^2\gamma_*^2} \tag{9}$$

$$\bar{E}_{xy} = \frac{1}{\sqrt{\Lambda_{11}\Lambda_{22}}} \frac{d}{2\sqrt{c_x c_y - d^2} + c_x\gamma + c_y\gamma_*}, \tag{10}$$

where $\gamma_*\gamma = 1$. Moreover,

$$\begin{aligned} c_x &= \Lambda_m + \Delta\Lambda\cos 2\phi \\ c_y &= \Lambda_m - \Delta\Lambda\cos 2\phi \\ d &= -\sin 2\phi\,\Delta\Lambda, \end{aligned}$$

with

$$\begin{aligned} \Lambda_m &= (\Lambda_1 + \Lambda_2)/2 \\ \Delta\Lambda &= (\Lambda_2 - \Lambda_1)/2. \end{aligned}$$

Equation (7) completely describes the flow dynamics occurring inside the inclusion. It allows the effective flow $\langle J\rangle$ to be derived as superposition of the base flow $(-\mathbf{\Lambda}\nabla p + \mathbf{\Gamma} U_m)$, the flow which would have been obtained without the inclusion (i.e., when the domain was constituted by the medium), and the flow difference introduced by the presence of the inclusion inside the medium $(-d\mathbf{\Lambda}\nabla p + d\mathbf{\Gamma} U_m)$:

$$\begin{aligned}\langle J\rangle &= -\mathbf{\Lambda}_{\text{eff}}\nabla p + \mathbf{\Gamma}_{\text{eff}} U_m \\ &= -\mathbf{\Lambda}\nabla p + \mathbf{\Gamma} U_m - d\mathbf{\Lambda}\nabla p + d\mathbf{\Gamma} U_m,\end{aligned} \tag{11}$$

where the effective flow conductivities $\mathbf{\Lambda}_{\text{eff}}$ and $\mathbf{\Gamma}_{\text{eff}}$ are, respectively, the effective Poiseuille and Couette conductivity tensors. Finally, according to the BEM approach, by replacing $\mathbf{\Lambda} = \mathbf{\Lambda}_{\text{eff}}$ and $\mathbf{\Gamma} = \mathbf{\Gamma}_{\text{eff}}$ in Eq. (11), and by using Eq. (7), the following couple of tensorial effective equations is obtained:

$$\langle d\mathbf{\Lambda}(\mathbf{I} + \mathbf{E}_0 d\mathbf{\Lambda})^{-1}\rangle = 0, \tag{12}$$

$$\langle d\mathbf{\Lambda}(\mathbf{I} + \mathbf{E}_0 d\mathbf{\Lambda})^{-1} d\mathbf{\Lambda}^{-1} d\mathbf{\Gamma}\rangle = 0, \tag{13}$$

where the notation $\langle\phi\rangle$ corresponds to $\langle\phi\rangle = c_i\phi_i$, and c_i is the area density of the generic ith component. From Eqs. (12) and (13), the conductivities $\mathbf{\Lambda}$ and $\mathbf{\Gamma}$ can be determined as a function of the texture conductivities $\mathbf{\Lambda}_\phi$ and $\mathbf{\Gamma}_\phi$ of each component.

Finally, the BEM lubrication problem $\nabla \cdot \langle J\rangle = 0$ is

$$\nabla \cdot [-\mathbf{\Lambda}\nabla p + \mathbf{\Gamma} U_m] = 0. \tag{14}$$

We are now interested in determining the average (effective) shear stresses. The local fluid shear stress, acting on the lower surface, is

$$\boldsymbol{\tau} = -\frac{\mathbf{v}_0\eta}{u(x) + l(x)} - \frac{1}{2}\left[1 + \frac{l(x)}{u(x) + l(x)}\right] u(x)\nabla p(x). \tag{15}$$

By averaging Eq. (15), the effective shear stress is

$$\langle\boldsymbol{\tau}\rangle = -\frac{\mathbf{v}_0}{\eta_0}\left\langle\frac{\eta/\eta_0}{u + l}\right\rangle - \frac{1}{2}\left\langle\left(1 + \frac{l}{u + l}\right) u\nabla p\right\rangle,$$

where $\langle(\eta/\eta_0)/(u + l)\rangle$ can be easily calculated from the texturing characteristics (e.g., in the case of shear-thinning lubricant, η/η_0 can be linked to the shear rate occurring at the inclusion level), η_0 is a reference fluid viscosity (e.g., the low-pressure, low-shear viscosity value), and where $\langle[1 + l/(u + l)]\, u\nabla p\rangle$ can be determined from Eq. (7).

In order to compare with existing full-scale numerical calculations, the effective Eqs. (12) and (13) are now solved in the simplest case of a two-component surface where circular inclusions are embedded in an isotropic medium; i.e., $\gamma = 1$ for both components. This results in isotropic effective conductivities, i.e., $\mathbf{\Lambda} = \Lambda\mathbf{I}$ and $\mathbf{\Gamma} = \Gamma\mathbf{I}$ (we confuse the tensor $\mathbf{\Lambda}$ with its diagonal element Λ for ease of reading). Moreover, the no-slip boundary condition is assumed for both components; i.e., $l_i = 0$. From Eqs. (8)–(10) we get

$$\mathbf{E}_0 = \frac{1}{2\Lambda}\mathbf{I}, \tag{16}$$

whereas from Eqs. (12) and (16), we get

$$\left\langle\frac{\Lambda - \Lambda_\phi}{\Lambda + \Lambda_\phi}\right\rangle = 0, \tag{17}$$

where Λ_ϕ is the Poiseuille conductivity of each component; i.e., for the holes (or pillar structure) $\Lambda_\phi = \Lambda_h = h_h^3/12\eta$ and for the substrate $\Lambda_\phi = \Lambda_f = h_f^3/12\eta$. By manipulating Eq. (17), we get

$$\begin{aligned}\tilde{\Lambda} = \frac{\Lambda}{\Lambda_f} &= (2p_h - 1)\frac{\tilde{\Lambda}_h - 1}{2} \\ &+ \frac{1}{2}\sqrt{(1 - 2p_h)^2(\tilde{\Lambda}_h - 1)^2 + 4\tilde{\Lambda}_h},\end{aligned} \tag{18}$$

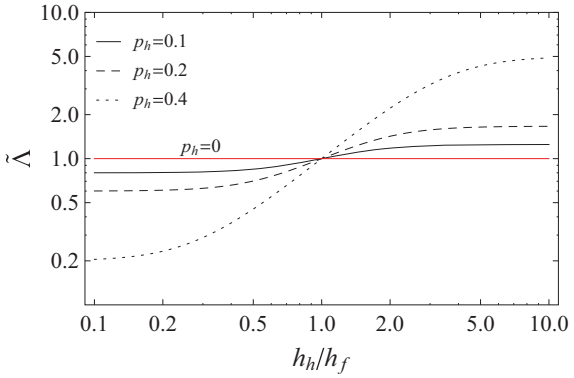

FIG. 4. (Color online) Pressure flow factor $\tilde{\Lambda}$ for circular inclusions embedded in an isotropic medium, as a function of the dimensionless hole ratio, and for different values of hole density p_h.

where $\tilde{\Lambda}_h = \Lambda_h/\Lambda_f = h_h^3/h_f^3$ in the case of constant fluid viscosity, and where p_h is the texture area density. From Eqs. (13) and (16) the effective Couette conductivity can be also determined:

$$\left\langle \frac{\Gamma_\phi - \Gamma}{\Lambda_\phi + \Lambda} \right\rangle = 0, \tag{19}$$

where Γ_ϕ is the Couette conductivity of each component, i.e., for the holes (or pillar structure) $\Gamma_\phi = \Gamma_h = h_h$ and for the substrate $\Gamma_\phi = \Gamma_f = h_f$. By manipulating Eq. (19), we get

$$\tilde{\Gamma} = \Gamma/\Gamma_f = \frac{\tilde{\Gamma}_h p_h(1+\tilde{\Lambda}) + (1-p_h)(\tilde{\Lambda}_h + \tilde{\Lambda})}{p_h(1+\tilde{\Lambda}) + (1-p_h)(\tilde{\Lambda}_h + \tilde{\Lambda})}, \tag{20}$$

where $\tilde{\Gamma}_h = \Gamma_h/\Gamma_f = h_h/h_f$. The effective fluid Eq. (14) simplifies then into

$$\nabla \cdot \left[\tilde{\Lambda} \frac{h_f^3}{12\eta} \nabla p \right] = \nabla \cdot \left[\tilde{\Gamma} h_f U_m \right], \tag{21}$$

where $\tilde{\Lambda}$ and $\tilde{\Gamma}$ correspond, respectively, to the pressure and shear flow factors for circular inclusions distributed in an isotropic medium. The pressure flow factor $\tilde{\Lambda}$ and the shear flow factor $\tilde{\Gamma}$, are shown, respectively, in Figs. 4 and 5 as a function of the dimensionless hole ratio h_h/h_f and for

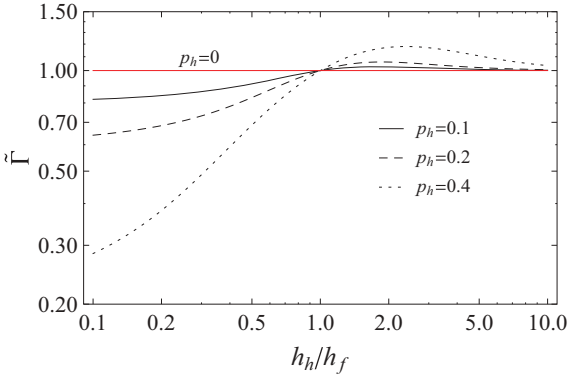

FIG. 5. (Color online) Shear flow factor $\tilde{\Gamma}$ for circular inclusions embedded in an isotropic medium, as a function of the dimensionless hole ratio, and for different values of hole density p_h.

different values of hole density p_h, respectively, $p_h = 0.1$, 0.2, 0.4. Values of $\tilde{\Lambda}$ (and of $\tilde{\Gamma}$) have been also calculated for pillar texturing, i.e., $h_h/h_f < 1$. Observe that the effective Poiseuille flow, which is proportional to $\tilde{\Lambda}$, is always bounded in between $(1-2p_h)$ and $(1-2p_h)^{-1}$ and in particular it is monotonically increasing with h_h/h_f. The effective Couette flow, proportional to $\tilde{\Gamma}$, shows instead a global maximum for $h_h/h_f \approx 2$. Interestingly, a further increase in the hole ratio determines a reduction of $\tilde{\Gamma}$, in particular to the value corresponding to the texture-free sliding. This is due to the appearance at the texture scale of local flows, generated by sliding-induced local pressure gradients, which are counteracting with respect to the sliding flow. Observe also that values of $\tilde{\Gamma} > 1$ correspond to an effective positive slippage on the textured surface, whereas in the case of pillar microstructures, for which $\tilde{\Gamma} < 1$, the effective predicted slippage is negative. Note that the effective slippage should be intended as occurring at both the generic inclusion scale (described by the local slip length l_h) as well as at the macroscale, where it results from the homogenization over multiple slippery (or not) inclusions, as discussed earlier in the paper. At the scale of the generic inclusion, however, the effective slip length l_h constitutes, together with the in-plane inclusion shape (i.e., ellipticity and a mayor axis direction), the local viscosity (η) and the out-of-plane projection (represented by h_h), the inclusion-effective characteristic. In particular, local slippage can be obtained by (subinclusion) chemical and/or physical modifications, e.g., by recurring to the nowadays widely used plasma process (see, e.g., Ref. [17]).

Equation (14) is now solved and the results compared to those of a three-dimensional partially textured lubrication problem (a thrust bearing macroscopic geometry) calculated, with a full-scale numerical resolution of Eq. (4), in a recently published paper [13]. In Fig. 6 we report the comparison, and, in particular, we show the BEM-homogenized fluid pressure (the smooth blue curve) in a bearing pad cross section, as

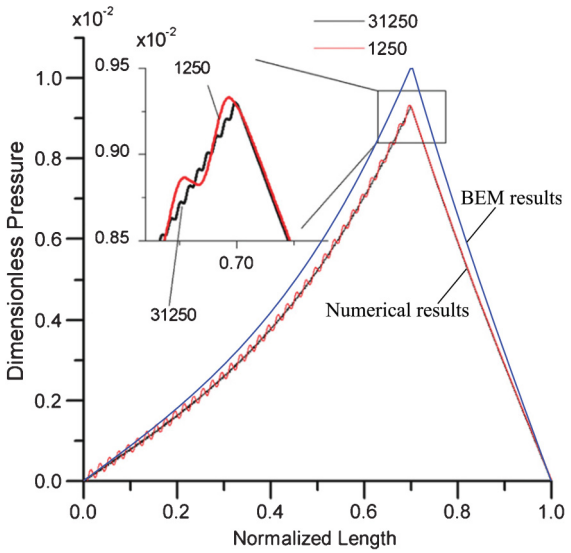

FIG. 6. (Color online) BEM-homogenized fluid pressure (the smooth blue curve) as a function of x coordinate (sliding direction), compared with the full scale numerical predictions partially adapted from Ref. [13].

compared to the numerical predictions of Ref. [13] (black and red curves). The latter curves have been calculated with the same texture areal density but with different hole in-plane size [13]. It is interesting to notice that, as confirmed by the full scale calculations, the local average fluid pressure is not dependent on the hole in-plane size but only on the texture areal density, in perfect agreement with our model. Moreover, observe the very good agreement between our predictions and the numerical results where differences must be mainly ascribed to the different hole geometry, squared in Ref. [13] and circular in our calculations. However, despite this difference, our model is very effective in providing an accurate estimation of the fluid pressure occurring in such a hydrodynamic contact. Our theory may be a very useful tool for the investigation of the surface texturing effects in the fluid dynamics occurring at the interface of sliding solids, e.g., for the near-optimum design of low friction hydrodynamic pairs.

[1] E. Stratakis, A. Ranella, and C. Fotakis, Biomicrofluidics **5**, 013411 (2011).

[2] I. Etsion, Tribol. Lett. **17**, 733 (2004).

[3] B. Persson, J. Chem. Phys. **115**, 3840 (2001).

[4] B. Persson, B. Lorenz, and A. Volokitin, Eur. Phys. J. E **31**, 3 (2010).

[5] M. Scaraggi, G. Carbone, B. Persson, and D. Dini, Soft Matter **7**, 10395 (2011).

[6] M. Scaraggi, G. Carbone, and D. Dini, Soft Matter **7**, 10407 (2011).

[7] B. Persson, J. Phys: Condens. Matter **22**, 265004 (2010).

[8] B. Persson and M. Scaraggi, Eur. Phys. J. E **34**, 113 (2011).

[9] A. Steinberger, C. Cottin-Bizonne, P. Kleimann, and E. Charlaix, Nat. Mater. **6**, 665 (2007).

[10] M. Sbragaglia and A. Prosperetti, J. Fluid Mech. **578**, 435 (2007).

[11] C.-O. Ng and C. Y. Wang, Fluid Dynam. Res. **43**, 065504 (2011).

[12] D. Bruggeman, Ann. Phys. **416**, 636 (1935).

[13] S. Pei, S. Ma, H. Xu, F. Wang, and Y. Zhang, Tribol. Int. **44**, 1810 (2011).

[14] M. Scaraggi, Tribol. Lett. (2012), doi: 10.1007/s11249-012-0025-6 (in press).

[15] S. Kirkpatrick, Rev. Mod. Phys. **45**, 574 (1973).

[16] P. Fokker, Transp. Porous Media **44**, 205 (2001).

[17] R. Di Mundo, F. Palumbo, and R. D'Agostino, Langmuir **26**, 5196 (2010).